Soft Matter

PAPER

View Article Online
View Journal | View Issue

Cite this: *Soft Matter*, 2016, 12, 4666

Interfacial free energy adjustable phase field crystal model for homogeneous nucleation

Can Guo, Jincheng Wang,* Zhijun Wang, Junjie Li, Yaolin Guo and Yunhao Huang

Received 31st March 2016,
Accepted 14th April 2016

DOI: 10.1039/c6sm00774k

www.rsc.org/softmatter

To describe the homogeneous nucleation process, an interfacial free energy adjustable phase-field crystal model (IPFC) was proposed by reconstructing the energy functional of the original phase field crystal (PFC) methodology. Compared with the original PFC model, the additional interface term in the IPFC model effectively can adjust the magnitude of the interfacial free energy, but does not affect the equilibrium phase diagram and the interfacial energy anisotropy. The IPFC model overcame the limitation that the interfacial free energy of the original PFC model is much less than the theoretical results. Using the IPFC model, we investigated some basic issues in homogeneous nucleation. From the viewpoint of simulation, we proceeded with an *in situ* observation of the process of cluster fluctuation and obtained quite similar snapshots to colloidal crystallization experiments. We also counted the size distribution of crystal-like clusters and the nucleation rate. Our simulations show that the size distribution is independent of the evolution time, and the nucleation rate remains constant after a period of relaxation, which are consistent with experimental observations. The linear relation between logarithmic nucleation rate and reciprocal driving force also conforms to the steady state nucleation theory.

1. Introduction

Nucleation of crystalline materials, the starting point for crystal formation from melts, has long been an important issue in condensed matter physics and materials science.[1–9] Nucleation plays a key role in determining the microstructures and mechanical properties of crystalline materials;[10–12] therefore, controlling nucleation is a very effective way for regulating the macrostructures of materials for specific applications. The process of nucleation, involving the fluctuation of short-range ordered structures and the formation of interfaces, is a dynamic process dominated by the competition between the reduced bulk free energy and the increased surface free energy. This competition constitutes the classical nucleation theory (CNT),[13,14] and gives rise to the conception of the nucleation barrier and the critical radius of nuclei. Although the CNT can explain experimental results well, the detailed dynamic process of nucleation is not totally clear, due to the lack of *in situ* observation techniques at atomic scales.

With the development of computer technology, computational simulation has been widely accepted as a third methodology in scientific research, complementing the traditional approaches of theory and experiment. Three modeling methods are widely adopted for the study of nucleation issues; *i.e.*, the phase field method (PFM),[15,16] molecular dynamics (MD) method[17,18] and kinetic Monte Carlo (KMC) method.[19,20] The PFM, a typical continuous model, has been widely used to simulate diffusive transport phenomena in solidification, such as nucleation and dendritic growth. However, since the atomic scale information is omitted in the PFM, a clear understanding of the atomic process of nucleation is impossible. The MD method is suitable for investigating phenomena that happen on atomic scales, but cannot operate on diffusive time scales, due to the limitations of computing resources. The KMC approach provides a method amenable to diffusive time scales, while incorporating some features of atomistic structure, but it currently lacks the ability to dynamically produce interface structure and strains associated with defects and solutes. Recently, a new method called the phase field crystal (PFC) model has been proposed to describe solidification issues.[21] The PFC model, as an atomic scale continuous field model, has been proposed to describe phenomena at the atomic length scale and the diffusive time scale, including elastic and plastic deformations in non-equilibrium processing, dislocation dynamics, crystal nucleation and growth, structure phase transformation,[22–26] *etc.*

Since the original PFC model was proposed, many nucleation issues have been investigated with this method. As early as 2007, R. Backofen *et al.*[27] introduced the PFC model to simulate the nucleation process. They also investigated the minimum energy path of homogeneous nucleation[28] and heterogeneous nucleation[29] with the string method. R. Prieler *et al.*[30,31] investigated the nucleation process with an anisotropic PFC model, and gave an overview on how the PFM and the PFC model can

State Key Laboratory of Solidification Processing, Northwestern Polytechnical University, Xi'an 710072, P. R. China. E-mail: jchwang@nwpu.edu.cn

be used to study nucleation from atomic to micro scales. Y. L. Guo *et al.*[32] studied the influence of noise strength on the nucleation process. L. Gránásy *et al.*[33,34] investigated amorphous nucleation precursors in high non-equilibrium fluids, nucleation at large undercooling and heterogeneous crystal nucleation in detail. M. A. Choudhary *et al.*[35] investigated the solid/liquid surface tension of critical nuclei and nucleation barriers with a binary alloy PFC model.

Although there are a series of simulation results about nucleation using the PFC method, some unresolved issues still exist. One of the most important problems is the absence of an atomic attachment/detachment process during the dynamic homogeneous nucleation process. Moreover, systematic work in building the connection between the PFC model and CNT is still lacking. The crux of the problem is the interfacial free energy of the PFC model. It has been proven that the solid/liquid interfacial free energy calculated by the original PFC model is about 20% smaller than that from CDFT and experiments.[23,36,37] As one of the most fundamental thermodynamic parameters governing phase transformations, the interfacial free energy plays a central role in determining the kinetics of crystal nucleation, crystal growth, equilibrium morphology, grain coarsening, and so on; thus, it is impossible to investigate solid/liquid transitions quantitatively by the original PFC model. To solve this problem, Jaatinen *et al.*[23] proposed an eighth-order fitting PFC model, and Asadi *et al.*[38,39] related the PFC parameters to the input data from MD simulations. Both the methods obtained relatively reasonable values for surface properties of bcc iron. However, as the PFC model is just a simplified CDFT, no matter how accurate the input parameters of the original PFC model are, the calculation results of interfacial free energy will be different with CDFT.

In this work, we first clarify the energy relation between the PFC model and CNT, and calculate the critical nuclei radius (r_c) of a one-component PFC model. Through the comparison of r_c, calculated by the original PFC model with the maximum size r_{max} of the short-range order cluster in an undercooled liquid, we demonstrate that r_c of the original PFC model is too small to describe the 'structure fluctuation' in a real nucleation process. This is due to the fact that the interfacial free energy of the original PFC model is smaller than the theoretical value. To solve this problem, we propose an interfacial free energy adjustable PFC model (IPFC), and check the effects of model parameters on solid/liquid interface properties and equilibrium thermodynamics properties. With the IPFC, the critical nuclei radius, snapshots of the pre-nucleation process at different evolution times, and nucleation rates are investigated in detail.

2. Model analysis

2.1 Classical nucleation theory

Nucleation from homogeneous undercooled liquids is initiated by the formation of clusters fluctuating in a crystal-like central atomic arrangement. The growth of these clusters depends on the competition between the decrease in bulk free energy, which contributes to growth, and the increase in interfacial free energy, which leads to shrinkage. Generally, clusters exceeding the critical size tend to grow, while clusters below the critical size will decay with a high probability. According to the two-dimensional (2D) CNT[14] for homogeneous nucleation, when a crystal-like cluster with a radius r is formed, the change in total free energy ΔG is,

$$\Delta G = -\pi r^2 \Omega \Delta G_B + 2\pi r \gamma l, \quad (1)$$

where ΔG_B is the difference in bulk free energy between the crystal phase and the liquid phase per unit, γ is the interfacial free energy (or line tension), Ω is the area per unit, and l is the length per unit. By solving $d(\Delta G)/dr = 0$, one can obtain the nucleation barrier (ΔG_c) and critical nuclei radius (r_c) as,

$$\Delta G_c = \frac{\pi \Omega \gamma^2 l^2}{\Delta G_B}, \; r_c = \frac{\Omega \gamma l}{\Delta G_B}. \quad (2)$$

2.2 The original PFC model

In the original PFC model, the simplest form of the free energy functional is as follows:[21]

$$\tilde{F} = \int \left[-|\nabla \psi|^2 + \frac{1}{2}(\Delta \psi) + f(\psi) \right] d\vec{r}, \quad (3)$$

where $f(\psi) = \frac{1}{2}(1-\varepsilon)\psi^2 + \frac{\psi^4}{4}$, ψ is the dimensionless time-averaged atom number density, and ε is a parameter related to temperature and crystal anisotropy. Another prevalent form of eqn (3) is $\tilde{F} = \int \left\{ \frac{\psi}{2}\left[-\varepsilon + \left(1+\nabla^2\right)^2 \right]\psi + \frac{\psi^4}{4} \right\} d\vec{r}$. The simulation parameters (ψ_0, ε) in this paper were chosen based on the 2-D phase diagram, where ψ_0 is the average atom number density. The dynamic equation is given by the following:

$$\frac{\partial \psi}{\partial t} = \Gamma \nabla^2 \frac{\delta \tilde{F}}{\delta \psi} + \eta, \quad (4)$$

where Γ is a mobility parameter, t is the dimensionless time, and η is a conserved stochastic noise. Here, η has the character of $\langle \eta(\vec{r}, t)\eta(\vec{r}', t') \rangle = -\xi \nabla^2 \delta(\vec{r} - \vec{r}')\delta(t - t')$, where ξ is the noise strength. Noise with a wavelength shorter than the interatomic spacing is filtered. This type of equation of motion is expected to be a good approximation in colloidal suspensions, where particle density relaxes diffusively *via* the Brownian motion of the particles. In this work, eqn (4) is solved using the semi-implicit Fourier spectral method, with a grid space of $dx = a/8$ and a time step of $dt = 0.5$, here a is the lattice constant. Parameters ψ_0 and ε in all our simulations are chosen in the coexistence region of liquid and solid phases.

2.3 Critical nuclei radius of the PFC model

Although the parameters in the PFC model have been linked to measurable quantities, the procedures for calculating critical nuclei radius from the PFC model are not straightforward, which is mainly due to the relationship between the PFC free energy and CNT not being fully developed. In this section, we present how to obtain ΔG_B, γ and the critical nuclei radius r_c, from PFC simulation. As a starting point, the dimensionless

bulk free energy ΔG_B for PFC can be calculated from the following equation:[26]

$$\Delta G_B = f_X(\psi_X) - \partial f_{liquid}/\partial\psi|_{\psi_0}(\psi_X - \psi_0) - f_{liquid}(\psi_0), \quad (5)$$

where ψ_X is the crystal density with a maximum driving force, f_X and f_{liquid} are the free energy densities for the solid and liquid phases respectively. The dimensionless interfacial free energy γ can be calculated as follows:[26,40]

$$\gamma = \frac{1}{L}\int \mathrm{d}r\left[f(r) - \left(f_s\frac{\psi-\bar{\psi}_l}{\bar{\psi}_s-\bar{\psi}_l} - f_l\frac{\psi-\bar{\psi}_s}{\bar{\psi}_s-\bar{\psi}_l}\right)\right], \quad (6)$$

where $f(r)$ is the free-energy density of the simulation system, $\bar{\psi}_l(\bar{\psi}_s)$ and $\bar{f}_l$ ($\bar{f}_s$) are the mean values of ψ and the free-energy density in liquid and solid phases, and L is the total length of the edge of the clusters.

With the dimensionless interfacial free energy γ, and bulk free energy ΔG_B, the critical nuclei radius r_c of PFC can be calculated exactly, according to the CNT. Here, r_c of a triangular phase has been calculated at temperature $\varepsilon = -0.3$. Fig. 1a shows the phase diagram of 2D PFC, for $\varepsilon = -0.3$, the coexistence region is $\psi_0 \in (0.312, 0.375)$. The driving force decreases with the increase in ψ_0. Fig. 1b shows the variation of r_c with different driving forces (ψ_0 = 0.33, 0.34, 0.35, 0.36, and 0.37). According to Fig. 1b, r_c increases with the decrease in driving force, which is consistent with the basic theory of solidification,[13,14] and the value of r_c changes from 0.6a to 2.4a. According to the CNT, only when the 'structure fluctuation' is larger than the critical nuclei, may the short-range ordered clusters have the chance to grow up. We then calculated the pair correlation function $g(r)$ to characterize the size of the 'structure fluctuations'. $g(r)$is defined as follows:

$$g(r) = 1 + \frac{1}{2\pi^2\rho_0 r}\int_0^\infty k(S(k)-1)\sin(kr)\mathrm{d}k \quad (7)$$

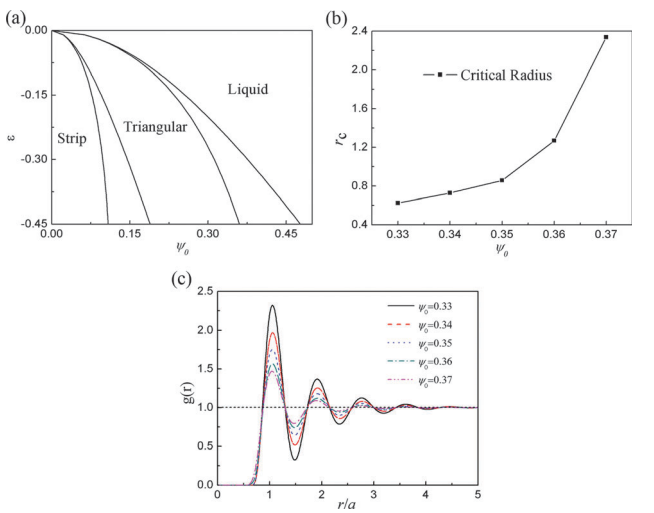

Fig. 1 (a) 2D phase diagram of the original PFC model; (b) critical nuclei radius r_c of different initial atom number densities ψ_0; (c) pair correlation function $g(r)$ with 5 different ψ_0, for ψ_0 = 0.33, 0.34, 0.35, 0.36 and 0.37.

where the structure factor $S(k)$ is defined in ref. 41 as $S(k) = \langle|\hat{\psi}_k|^2\rangle$, $\hat{\psi}_k = \int \mathrm{d}\vec{k}\psi(\vec{r})\mathrm{e}^{-\vec{k}\cdot\vec{r}}$. Fig. 1c shows $g(r)$ for five different ψ_0. The number of peaks of $g(r)$ reflects the maximum size of the cluster in liquid. By checking $g(r)$, we know that the possible maximum radial radius of a crystal-like cluster is about 3–4a near the melt point. With the decrease in driving force, both the number and the amplitude of peaks in $g(r)$ are decreased, which is consistent with the experimental results.[42] Comparing the results in Fig. 1b and c, the radius of the largest cluster (r_{max}) is much larger than the critical nuclei radius r_c when ψ_0 is less than 0.36. This means that almost all short-range order clusters in PFC modeling are larger than the critical nuclei, and favor growth. In particular, the value of r_c is even less than 1a near the melting point. In this case, any crystal-like clusters can grow up easily. However, this is impossible in real material systems. As for $\psi_0 > 0.36$, both the phase transition driving force and the final solid volume fraction of PFC are too small, as indicated in Fig. 1(a). In this case, the relaxation time of nucleation is too long, which makes the PFC inefficient to study the free nucleation issues; therefore, the original PFC is inadequate to study complex nucleation issues directly.

3. IPFC model

From the discussions above, the critical nucleation radius and the nucleation barrier in the original PFC model are too small, which is the main reason why the original PFC model is not suitable for studying general homogeneous nucleation processes. Any clusters originating from structure fluctuations in PFC simulation will grow up immediately, as shown in ref. 32. Thus, the application of the PFC model in describing the evolution process of the initial stage of nucleation of clusters is challenging. Eqn (2) shows that both r_c and ΔG_c are directly proportional to the ratio of γ to ΔG_B; these two parameters can be amended to correct for the nucleation barrier of the PFC model. In light of the fact that the interfacial free energy of PFC, γ, is much smaller than that obtained from CDFT and experimental results, we intend to construct an interfacial free energy adjustable PFC model to amend the nucleation barrier.

3.1 The building of IPFC

As the original PFC model is just a 'simplified version' of CDFT, all the higher-order gradient terms that affect the solid/liquid interface properties are omitted to improve its computational efficiency. This leads to the fact that the interfacial free energy is less than the experimental and theoretical results. One can improve the PFC model by precisely fitting the higher order gradient terms in CDFT; however, this will inevitably increase the complexity and lose the advantage of the high efficiency of the PFC model.[23,26,43] One also can amend this model by adding an interface term in its free energy functional, to compensate for the interfacial free energy missed, and it would be better if this additional interface term only affected the solid/liquid interfacial energy, but had no influence on the bulk

free energy. Here, we try to amend the interfacial free energy of the original PFC by adding an interface term.

As we know, the PFM is an excellent numerical method to figure out issues involving the solid/liquid interface. In the PFM, the free energy functional of the system is as follows:

$$F(\varphi) = \int \left[\frac{\delta}{2}|\nabla\varphi|^2 + \frac{1}{\delta}g(\varphi)\right]\mathrm{d}\vec{r}, \tag{8}$$

where φ is an order parameter, δ determines the width and strength of the interface, and $g(\varphi)$ is a double well potential. Comparing the free energy function of the PFC model with that of the classical PFM, both the free energy functionals of the PFC model and the PFM contain a double well potential, which determines whether both models can describe phase transition problems. The major differences between these two models are in the definition of order parameters and the interfacial free energy term. As in the solid phase, the order parameter of PFC fluctuates periodically, while it remains constant in the PFM. The interfacial free energy in the PFC model is implied in the gradient terms and coupled with the double well potential, while in PFM the interfacial free energy is independent and adjustable. Through fitting the coefficient δ, the magnitude of the interfacial free energy of the PFM can be in good agreement with experimental values. With a similar treatment in the Cahn–Hilliard theory, we added such a gradient term to modulate the interfacial free energy of the original PFC model. The simplified dimensionless one-component IPFC free energy functional is as follows:

$$\tilde{F} = \int \left\{\frac{\psi}{2}\left[-\varepsilon + \left(1+\nabla^2\right)^2\right]\psi + \frac{\psi^4}{4} + \frac{\alpha}{2}\left|\nabla\bar{\psi}\right|^2\right\}\mathrm{d}\vec{r}, \tag{9}$$

where α is a constant that affects the strength of the interfacial free energy, and $\bar{\psi} = \int \mathrm{d}\vec{r}\chi(\vec{r}-\vec{r}')\psi(\vec{r})$ is the local spatial average of the density field ψ, with χ as the local smoothing kernel,[44] where $\chi(k) = \exp(-k^2/2\lambda)$ in Fourier space. χ affects low k modes, only picking up density contributions at long wavelengths, and the parameter λ affects the surface energy. For a one-component system, $\bar{\psi}$ will be constant in both the solid phase and liquid phase, and the gradient term in eqn (9) will be zero. Thus, this interfacial term only works in the region of the interface, and does not affect the equilibrium properties of the model. Moreover, the phase diagram of IPFC should have no difference from that in the original PFC model, and the character of high computational efficiency of the original PFC model is also inherited by our IPFC. We noticed that Schwalbach *et al.*[45] proposed a similar approach to regulate the interface properties. In their two-field model, they introduced an additional phenomenological non-conserved order parameter to characterize the vapor phase, condensed phase and interface, and the vapor/condensed interfacial free energy can be modified by varying the parameters in the free energy functional. Compared with their model, our approach is simpler. The dynamic equation of the IPFC model can be given as follows:

$$\frac{\partial\psi}{\partial t} = \Gamma\nabla^2\left[\left(-\varepsilon + \left(1+\nabla^2\right)^2\right)\psi + \psi^3 + E_\mathrm{r}\right] + \eta, \tag{10}$$

where $E_k = \alpha k^2 \exp(-k^2/\lambda)\hat{\psi}$ is the Fourier form of E_r (see Appendix for the details of arriving at eqn (10)). This dynamic equation is solved using the semi-implicit Fourier spectral method.

3.2 The effect of the interface term in the IPFC model

In this section, we will discuss the effect of the interface term in the IPFC model on the system's equilibrium thermodynamic properties and interface properties. The size of the simulation box is: $L_x \times L_y = 1024 \times 64$. Crystallization is started by placing a rectangular slab filled with the density field of triangular structure at the center of the simulation box, where the density field of triangular structure can be represented by $\psi_\mathrm{tri} = A\left[\cos(q_0 x)\cos\left(q_0 y/\sqrt{3}\right) - \cos\left(2q_0 y/\sqrt{3}\right)/2\right] + \psi_0$, where A is an unknown constant and $q_0 = 2\pi/a$; the crystal grows along the x-axis.

3.2.1 The effect on the equilibrium properties. To confirm that the interface term in the IPFC model does not affect the equilibrium properties, we mainly examined whether the mean atom density is equal to the PFC model when the two phases are coexisting in equilibrium. Table 1 shows the mean atomic density of $\bar{\psi}_\mathrm{l}$ and $\bar{\psi}_\mathrm{s}$ with different initial densities ψ_0 and the parameter α, where the data for $\alpha = 0$ corresponds to the result of the original PFC model. All these data are obtained from our simulation results. According to Table 1, the density difference between the IPFC and PFC models is less than 0.5%, thus, the interface term in IPFC has no influence on the equilibrium density. As a result, all the phase diagrams calculated by the original PFC model can be used in IPFC.

3.2.2 The effect on the interface properties. In this section, we will check the impact of the interface term on the interfacial free energy, the interface dynamic properties, the interface width, and the anisotropy of the interface. The interfacial free energy γ is calculated by eqn (6) after the system is relaxed to solid–liquid equilibrium. Fig. 2a shows the interfacial free energy of γ_a and γ_b for $\psi_0 = 0.35$ with different α, where the subscript a (b) represents the crystal face perpendicular to the a (b) axis shown as the inset. Fig. 2b shows the rate of change $((\gamma - \gamma_0)/\gamma_0)$ of γ_a and γ_b. According to Fig. 2a, we know that γ increases with the increase in α for both the crystal faces, and γ is almost doubled when $\alpha = 100$. This means that our original purpose of regulating γ is fulfilled. According to Fig. 2b the

Table 1 Two phases of equilibrium coexist, densities $\bar{\psi}_\mathrm{l}$ and $\bar{\psi}_\mathrm{s}$ with different interfacial coefficients α (from 0 to 100), and super saturation of ψ_0 (from 0.33 to 0.36, and with $\alpha = 20$), the data for $\alpha = 0$ correspond to the result of the original PFC model

α	0	20	40	70	100	ψ_0	0.33	0.34	0.35	0.36
$\bar{\psi}_\mathrm{l}$	0.3776	0.3781	0.3778	0.3771	0.3761		0.3790	0.3783	0.3781	0.3780
$\bar{\psi}_\mathrm{s}$	0.3145	0.3155	0.3154	0.3151	0.3144		0.3166	0.3157	0.3155	0.3153

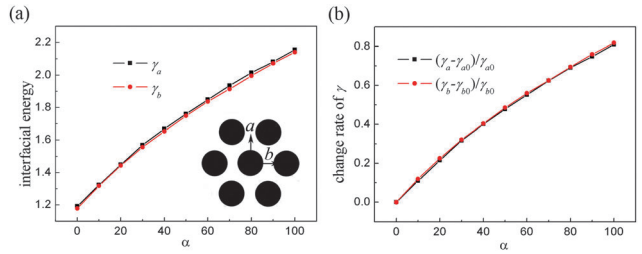

Fig. 2 (a) The interfacial free energy of the crystal face perpendicular to orientation *a* (γ_a) and *b* (γ_b) *vs.* α, where α is the coefficient of the interface term. (b) The rate of change of $\gamma_a(\gamma_b)$ *vs.* α.

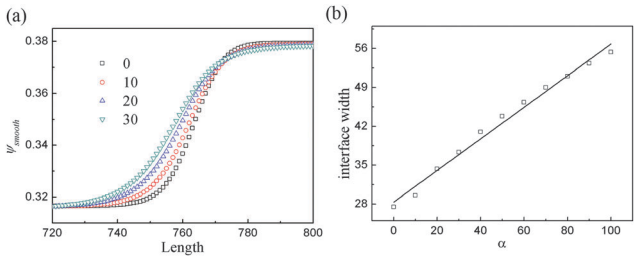

Fig. 4 (a) The smoothing density across the solid/liquid interface with α= 0, 10, 20, 30. (b) The width of the solid/liquid interface with α = 0, 10, 20,...100.

rates of change of γ_a and γ_b are almost same (the difference is less than 2%), which indicates that the interface term does not affect the interfacial free energy anisotropy. Actually, the interfacial free energy anisotropy can be regulated through replacing the operator of the IPFC model by a more general differential operator to allow the spatial anisotropy, as is done in ref. 30.

Fig. 3a shows the variation of interface position (Z) *versus* evolution time (τ) for crystal orientations parallel to the *a* and *b* axes. After a short time, the interface position Z roughly displays a $Z \propto \tau^{1/2}$ behavior, indicating a diffusion-controlled growth mechanism. This kind of behavior is often observed in colloidal systems,[46] which is also the same with results from the original PFC model.[26,47] To obtain the dynamic coefficient, we fit the interface position and time relationship with the function $Z = Z_0 + C(\tau + \tau_0)^{1/2}$, where Z_0 is the initial interface position, C is the interface velocity coefficient, and τ_0 is the transient time. Fig. 3b shows the interface velocity coefficient for *a* and *b* orientations. According to Fig. 3b, we can see that for $(\psi_0, \varepsilon) = (0.35, -0.3)$ the growth velocity C_a and C_b are nearly equal, which is consistent with the results of the original PFC model of Tang *et al.*[22] Moreover, both C_a and C_b are approximately equal to 1.02 (the difference is less than 5%), and do not change with α.

Fig. 4a shows the smoothing density across the solid/liquid interface with different α, while Fig. 4b shows the width (W) of the solid/liquid interface. According to Fig. 4a, the transition between $\bar{\psi}_s$ (crystal phases) and $\bar{\psi}_l$ (liquid phase) is gentler, and the size of the transition zone increases with the increase of α.

This means that the interface term can affect the interface width (W), and the relation of W *vs.* α is shown in Fig. 4b. For α = 100, W is almost doubled. Similar to the phase field model, the free energy functional of the IPFC model is also constructed by a double well potential and a gradient term. Since $\bar{\psi}$ is a local spatial average of the density field, the gradient term in the IPFC model only affects the energy at the interface. When the interface term is added, the energy of a sharp interface will be larger than the energy of a dispersive interface, which is why the strength of the interface term in the IPFC model can affect the interface width.

We have discussed the effect of the interface term on the interfacial properties under the same driving force above. Further, we investigated the effect of this interface term on the interfacial free energy and the interface velocity coefficient under different driving forces. Fig. 5a shows the interfacial free energy γ_a, γ_b, γ_{a0}, γ_{b0}, $(\gamma_a - \gamma_{a0})/\gamma_{a0}$ and $(\gamma_b - \gamma_{b0})/\gamma_{b0}$ for α = 0 and 20, with different initial atom densities ψ_0, ψ_0 = 0.335, 0.34,...0.36, where the corner mark '0' in γ_{a0} (γ_{b0}) corresponds to α = 0. Fig. 5b shows the interface velocity coefficient of *a* and *b* orientation *vs.* ψ_0. For both α = 0 and 20, increasing ψ_0 (decrease of driving force), increases the interfacial energy, while the interface velocity coefficient is decreased. This tendency conforms to the original PFC model.[22] From Fig. 5a, we know that as α increases from 0 to 20, the rate of change of the interfacial free energy is around 25% for all six ψ_0. Thus, the impact of α on the interfacial energy is independent of ψ_0. However, the impact of α on the interface velocity coefficient depends on ψ_0, as shown in Fig. 5b. The smaller the ψ_0, the greater the impact of the

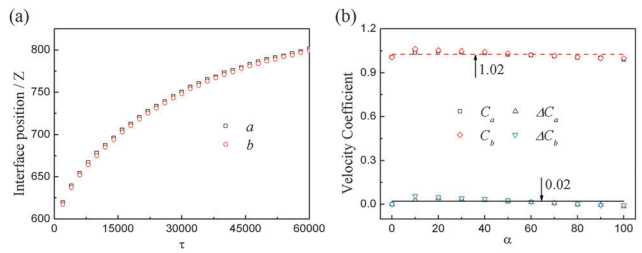

Fig. 3 (a) The interface position (Z) *vs.* time (τ) for two different crystallographic orientations (*a* and *b*), where α = 60. (b) The interface dynamic coefficient for *a* and *b* orientations, where □ represents the coefficient of the *a* orientation (C_a), ◊ represents the coefficient of the *b* orientation (C_b), △ is the rate of change of C_a compared with C_{a0} ($\Delta C_a = (C_a - C_{a0})/C_{a0}$), ▽ is the rate of change of C_b (ΔC_b), C_{a0} is the dynamic coefficient for α = 0.

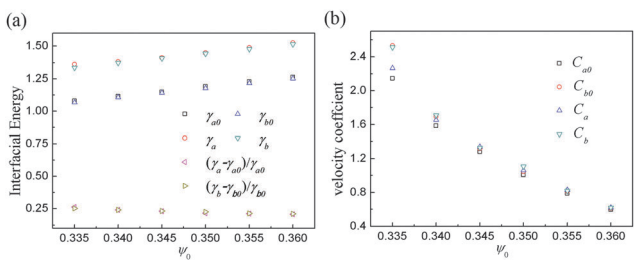

Fig. 5 (a) The interfacial free energy γ_a, γ_b, γ_{a0}, γ_{b0}, $(\gamma_a - \gamma_{a0})/\gamma_{a0}$ and $(\gamma_b - \gamma_{b0})/\gamma_{b0}$ for α = 0, 20, with ψ_0 = 0.335, 0.34,...0.36, where the corner mark '0' corresponds to α = 0; (b) the interface velocity coefficient of *a* and *b* orientation *vs.* ψ_0.

interface term on the velocity coefficient and kinetic anisotropy. Tang *et al.*[22] investigated the atom stacking mechanism under different undercooling conditions using the original PFC model. For a weak undercooling, crystal growth is under diffusion-controlled mode, and the interface term in IPFC has a tiny effect on the kinetic properties, while for a large undercooling, crystal growth is no longer diffusion controlled. Under this condition, the change of interface width will affect the atom stacking process, and the kinetic properties will be affected.

Above all, we discuss the effect of the interface term in the IPFC model on the equilibrium properties and interface properties. Simulation results show that the interface term does not affect the equilibrium phase diagram or interfacial free energy anisotropy. The main impact of this term is on the magnitude of the solid/liquid interfacial free energy and the width of the interface. It should be noted that for a large driving force, the interface term would affect the velocity coefficient and the kinetic anisotropy.

4. Homogeneous nucleation process simulated by the IPFC model

In this section, we investigate the 2D homogeneous nucleation process with the IPFC model. Nucleation in the undercooled liquids is induced by stochastic noises. The size of our simulation box is a $L_x \times L_y = 1024 \times 1024$ grid, the noise strength is $\eta = 0.0003$, and the interface term coefficient is $\alpha = 20$. In order to guarantee the reliability of the simulation results, all the data in this section are obtained from 5 simulations.

Fig. 6a–c shows a typical pre-nucleation and post-nucleation process for $(\psi_0, \varepsilon) = (0.35, -0.3)$, which includes the evolution of cluster fluctuation in the initial stages and the formation of stable nuclei. Fig. 6d–f shows the same stage of nucleation as the colloid experiment by Liu *et al.*[48] In both our simulation and in ref. 48, the crystal-like atoms are highlighted by bright (colored blue) spheres, and only those with density amplitude larger than 0.85 $A_{eq.}$ ($A_{eq.}$ is the equilibrium amplitude of the triangle phase) are treated as crystal-like atoms in our simulation. The clusters in the red circle kept on growing, while the clusters in the yellow circle disappeared quickly. This stochastic fluctuation of clusters is similar in all of our five simulations, and such types of fluctuations last until the nucleation source is depleted. Through a simple comparison of Fig. 6a–c with Fig. 6d–f, the nucleation process of the IPFC model is consistent with the colloid experiments, which verifies that our IPFC model can describe the fluctuation in the homogeneous nucleation of the clusters.

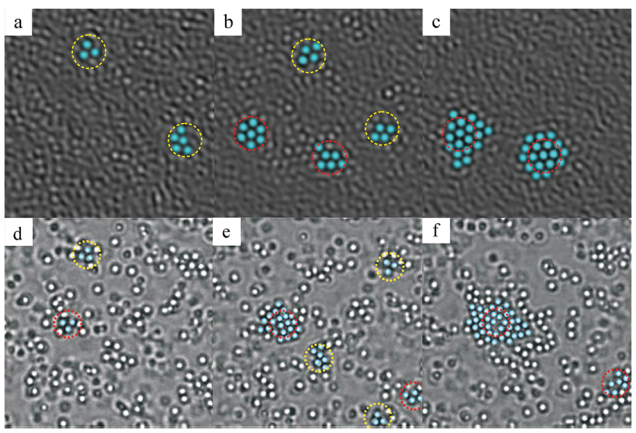

Fig. 6 Snapshots of the initial stage of nucleation at different times, where the radius of the circles equals the critical nuclei radius. The bright (colored blue) spheres are crystal-like atoms; our simulation results are (a) 2000Δt, (b) 3000Δt, (c) 5000Δt; (d–f) are the experimental results of Liu *et al.*[43] (reproduced with permission from Ke-Qin Zhang and Xiang Y. Liu. *In situ* observation of colloidal monolayer nucleation driven by an alternating electric field; *Nature*, 2004, **429**, 6993, ©2004 by Nature Publishing Group).

Fig. 7a shows the size distribution (N_n) of 2D crystalline clusters at different evolution times, where n is the atom number of these clusters. When $t = 3000\Delta t$, the size distribution approaches a steady state, where N_n is independent of time. In the CNT, the equilibrium size distribution N_n^* can be estimated by a Boltzmann distribution $N_n^* = N_1 \exp(-\Delta G_n/k_B T)$, where N_1 is the number of liquid atoms, ΔG_n is the free energy of the crystal-like cluster, k_B is the Boltzmann constant, and T is temperature. For the 2D nucleation theory, $\Delta G_n = 2\gamma l(\pi\Omega n)^{1/2} - n\Delta G_B$. The atom number of the critical nuclei is about 6, from theoretical calculations. However, the critical nuclei contain about 8 atoms based on our simulations (Fig. 7a), which is a little bit larger than the theoretical calculation value. This is mainly due to the fact that the clusters in the real nucleation process are not a norm circle, so the area of the interface is always larger than that in the theory model, which will enlarge the potential barrier. Thus, the clusters would need more atoms to gather together to overcome the nucleation potential barrier. Although the shapes for most of the clusters are not regular, the cluster evolution mechanisms of our IPFC simulations are same as the CNT. Our simulation results about the size distribution *vs.* time contain the transformation from the transition state to steady state, which is in line with the general rules of the experiment and theory.[13,14,48] The size distribution of our simulation is lower than the equilibrium state distribution N_n^*. It comes close to N_n^* only as the cluster size n approaches 1, which is owing to the fact that crystal nuclei continue to grow up. In Fig. 7b, we counted the number of clusters (N_g), which is larger than the critical nuclei for $t \geq 3000\Delta t$, corresponding to the moment that they reach the steady state of size distribution. The slope of the size distribution (N_g) curve is the nucleation

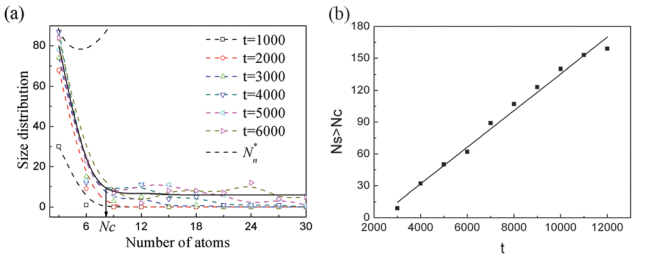

Fig. 7 (a) The size distribution of crystal-like clusters at different times, N_c is the atom number of critical nuclei; (b) the number of nuclei larger than the critical size *vs.* evolution time.

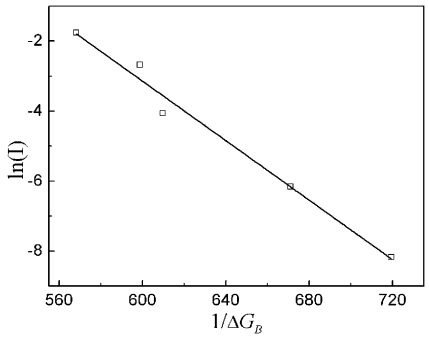

Fig. 8 The nucleation rate *versus* driving force of IPFC.

rate; a constant slope corresponds to the steady nucleation rate I, which means that new crystal nuclei form continually and the post-nucleation crystals grow up continuously. This is why N_n is a horizontal line with respect to the n axis after relaxation. When $t > 10\,000\Delta t$, the nucleation rate will decrease with time, and the liquid atoms are more inclined to attach to the existing crystal nuclei. The decrease in nucleation rate is mainly caused by the decrease of the crystallization driving force in a continuous crystal growth system.

To characterize the nucleation kinetic feature, we calculated the steady-state nucleation rate, which is the number of newly added crystal nuclei per unit time and per unit area. Here, we counted the nucleation rate for 5 different driving forces. For stationary conditions, the theoretical prediction of the nucleation rate depends on the following relation:

$$I = N_0 B \exp(-W_*/k_B T), \tag{11}$$

where W_* is the critical crystalline nucleus formation, N_0 is the number of atoms in a unit volume of the liquid, and B is a kinetic factor. For low-viscosity melts, B changes insignificantly with the change in undercooling, therefore, in the PFC system, B can be treated as a constant. Here, for 2D nucleation, $W_* = W_c$. The relationship between $\ln(I)$and $1/\Delta G_B$ is shown in Fig. 8. It shows that the nucleation rate decreases with the decrease in driving force, and the significant linear relationship between $\ln(I)$ and $1/\Delta G_B$ is consistent with the steady state kinetics of 2D nucleation theories and colloid experimental results.[13,14,48–50]

5. Conclusions

In summary, an interfacial energy adjustable phase field crystal (IPFC) model was proposed based on the original PFC model and the PFM. Through calculation analysis, we verified that the additional interface term in the IPFC model does not affect the basic properties of the original PFC model, such as the equilibrium phase diagram, and interfacial energy anisotropy. The main impact of this term is on the magnitude of the solid/liquid interfacial free energy and the width of the interface. The interfacial free energy will increase with the increase of the interface term. The limitation that the interfacial energy of the original PFC model is much smaller than the theoretical results can be overcome by the IPFC model. Further, we clarified the free energy relation between the PFC model and the CNT, and checked the critical nuclei radius of the one-component PFC model. With the IPFC model, we conducted an *in situ* observation of the process of the clusters' fluctuations from the viewpoint of simulation, and our simulation results are quite similar to the colloidal crystallization experiments. We also counted the size distribution of crystal-like clusters *vs.* time, and calculated the nucleation rate *vs.* different driving forces. Our simulation results revealed the general rule of nucleation, and are consistent with the classical 2D nucleation theory and experimental studies. The validity of our IPFC on the study of nucleation problems is well proven, and more detailed and systematic investigations would help us to understand the nucleation mechanism better. Although this IPFC model was proposed to solve nucleation issues initially, this interfacial free energy adjustable model is also useful in the study of other solidification problems, such as grain coarsening, dendritic growth, and so on.

Appendix: numerical method

We start by defining $\psi_D = \nabla\int dr\chi(r-r')\psi = \nabla(\chi\times\psi) = (\nabla\chi)\times\psi = \chi_D\times\psi$ and rewriting the free energy functional of the IPFC model as follows:

$$\tilde{F} = \int\left\{\frac{\psi}{2}\left[-\varepsilon + \left(1+\nabla^2\right)^2\right]\psi + \frac{\psi^4}{4} + \frac{\alpha}{2}{\psi_D}^2\right\}d\vec{r}. \tag{A1}$$

When computing $\delta\tilde{F}/\delta\psi$, the term with ψ_D is $\alpha\chi_D\times\psi_D$, and the chemical potential can be written as follows:

$$\frac{\delta\tilde{F}}{\delta\psi} = \left(-\varepsilon + \left(1+\nabla^2\right)^2\right)\psi + \psi^3 + \alpha\chi_D\times(\chi_D\times\psi) + \eta, \tag{A2}$$

the convolution is

$$\chi_D\times\psi = FT\{\chi_{Dk}\psi_k\}, \tag{A3}$$

where the corner mark 'k' designates the Fourier formalism of the terms, $FT\{\}$indicates the Fourier transform of the term in brackets. Eqn (10) is discretized and solved numerically with a semi-implicit spectral technique using a discrete time step Δt. The linear terms are implicitly evaluated at $t+\Delta t$, while all the non-linear terms are evaluated at time t. If we define

$$c = [1 + \Gamma k^2\Delta t(-\varepsilon + (1-k^2)^2 + \alpha(k\chi)^2)]^{-1}, \tag{A4}$$

$$b = -\Gamma\Delta t k^2, \tag{A5}$$

then the discretization evolution function is,

$$\psi_k^{t+\Delta t} = c[\psi_k^t + b(FT\{\psi^3\})]. \tag{A6}$$

Acknowledgements

This work is supported by National Natural Science foundation of China (Grant No. 51571165, 51371151), Supported by the Fundamental Research Funds for the Central Universities 3102015BJ(II)ZS001 and Free Research Fund of State Key Laboratory of Solidification Processing (100-QP-2014). We also thank the Center for High Performance Computing of

Northwestern Polytechnical University, China for computer time and facilities.

References

1 R. Blaak, S. Auer, D. Frenkel and H. Löwen, *Phys. Rev. Lett.*, 2004, **93**, 068303.
2 K. Lu and Y. Li, *Phys. Rev. Lett.*, 1998, **80**, 20.
3 K. A. Fichthorn and M. Scheffler, *Phys. Rev. Lett.*, 2000, **84**, 23.
4 W. J. Boettinger and S. R. Coriell, *Acta Mater.*, 2000, **48**, 43–70.
5 T. E. Quested and A. L. Greer, *Acta Mater.*, 2005, **53**, 2683–2692.
6 A. Engelbrecht, R. Meneses and H. J. Schöpe, *Soft Matter*, 2011, **7**, 5685–5690.
7 M. Franke, A. Lederer and H. J. Schöpe, *Soft Matter*, 2011, **7**, 11267–11274.
8 J. Diemand, R. Angélil, K. K. Tanaka and H. Tanaka, *Phys. Rev. E: Stat., Nonlinear, Soft Matter Phys.*, 2014, **90**, 052407.
9 W. K. Qi, Y. Peng, Y. L. Han, R. K. Bowles and M. Dijkstra, *Phys. Rev. Lett.*, 2015, **115**, 185701.
10 A. Cuetos, R. van Roij and M. Dijkstra, *Soft Matter*, 2008, **4**, 757–767.
11 Y. Liu, Y. Zhang, W. H. Yu, X. T. Wang, H. L. Zheng and X. L. Tian, *Scr. Mater.*, 2016, **110**, 87–91.
12 J. W. Schmelzer, J. Schmelzer Jr and I. S. Gutzow, *J. Chem. Phys.*, 2000, **112**, 3820.
13 P. G. Debenedetti, *Metastable Liquids*, Princeton University Press, Princeton, Concepts and Principles, 1996.
14 J. W. P. Schmelzer, *Nucleation Theory and Applications*, WILEY-VCH Verlag GmbH & Co. KGaA, Concepts and Principles, 2004.
15 B. Nestler and A. A. Wheeler, *Phys. Rev. E: Stat. Phys., Plasmas, Fluids, Relat. Interdiscip. Top.*, 1998, **57**, 2602.
16 W. J. Boettinger, J. A. Warren, C. Beckermann and A. Karma, *Annu. Rev. Mater. Res.*, 2002, **32**, 113.
17 Z. G. Xia, D. Y. Sun, M. Asta and J. J. Hoyt, *Phys. Rev. B: Condens. Matter Mater. Phys.*, 2007, **75**, 012103.
18 M. Asta, C. Beckermann, A. Karma, W. Kurz, R. Napolitano, M. Plapp, G. Purdy, M. Rappaz and R. Trivedi, *Acta Mater.*, 2009, **57**, 941.
19 E. Clouet, M. Nastar and C. Sigli, *Phys. Rev. B: Condens. Matter Mater. Phys.*, 2004, **69**, 064109.
20 S. Auer and D. Frenkel, *Annu. Rev. Phys. Chem.*, 2004, **55**, 333–361.
21 K. R. Elder, M. Katakowski, M. Haataja and M. Grant, *Phys. Rev. Lett.*, 2002, **88**, 245701; K. R. Elder and M. Grant, *Phys. Rev. E: Stat., Nonlinear, Soft Matter Phys.*, 2004, **70**, 051605.
22 S. Tang, Y. Yu, J. Wang, J. Li, Z. Wang, Y. Guo and Y. Zhou, *Phys. Rev. E: Stat., Nonlinear, Soft Matter Phys.*, 2014, **89**, 012405.
23 A. Jaatinen, C. V. Achim, K. R. Elder and T. Ala-Nissila, *Phys. Rev. E: Stat., Nonlinear, Soft Matter Phys.*, 2009, **80**, 031602.
24 M. Greenwood, N. Provatas and J. Rottler, *Phys. Rev. Lett.*, 2010, **105**, 045702.
25 K. Wu, A. Adland and A. Karma, *Phys. Rev. E: Stat., Nonlinear, Soft Matter Phys.*, 2010, **81**, 061601.
26 C. Guo, J. C. Wang, Z. J. Wang, J. J. Li, Y. L. Guo and S. Tang, *Phys. Rev. E: Stat., Nonlinear, Soft Matter Phys.*, 2015, **92**, 013309.
27 R. Backofen, A. Rätz and A. Voigt, *Philos. Mag. Lett.*, 2007, **87**, 813–820.
28 R. Backofen and A. Voigt, *J. Phys.: Condens. Matter*, 2010, **22**, 364104.
29 R. Backofen and A. Voigt, *Eur. Phys. J.: Spec. Top.*, 2014, **223**, 497–509.
30 R. Prieler, J. Hubert, D. Li, B. Verleye, R. Haberkern and H. Emmerich, *J. Phys.: Condens. Matter*, 2009, **21**, 464110.
31 R. Prieler, D. Li and H. Emmerich, *J. Cryst. Growth*, 2010, **312**, 1434–1436.
32 Y. L. Guo, J. C. Wang, Z. J. Wang, S. Tang and Y. H. Zhou, *Acta Phys. Sin.*, 2012, **61**, 146401.
33 G. Tegze, G. I. Tóth and L. Gránásy, *Phys. Rev. Lett.*, 2011, **106**, 195502.
34 L. Gránásy, G. Tegze, G. I. Tóth and T. Pusztai, *Philos. Mag.*, 2011, **91**, 123–149.
35 M. A. Choudhary, J. Kundin, H. Emmerich and M. Oettel, *Phys. Rev. E: Stat., Nonlinear, Soft Matter Phys.*, 2014, **90**, 022403.
36 M. Oettel, S. Dorosz, M. Berghoff, B. Nestler and T. Schilling, *Phys. Rev. E: Stat., Nonlinear, Soft Matter Phys.*, 2012, **86**, 021404.
37 E. Asadi and M. A. Zaeem, *JOM*, 2015, **67**, 186–201.
38 E. Asadi, M. A. Zaeem, S. Nouranian and M. I. Baskes, *Phys. Rev. B: Condens. Matter Mater. Phys.*, 2015, **91**, 024105.
39 E. Asadi and M. A. Zaeem, *Comput. Mater. Sci.*, 2015, **105**, 101–109.
40 K. Wu and A. Karma, *Phys. Rev. B: Condens. Matter Mater. Phys.*, 2007, **76**, 184107.
41 N. Provatas, K. Elder, *Phase Field Methods in Material Science and Engineering*, WILEY-VCH, 2007.
42 Y. Waseda, *The Structure of Non-Crystalline Materials Liquids and Amorphous Solids*, McGraw-Hill Inc, American, 1980.
43 N. Pisutha-Arnond, V. W. L. Chan, M. Iyer, V. Gavini and K. Thornton, *Phys. Rev. E: Stat., Nonlinear, Soft Matter Phys.*, 2013, **87**, 013313.
44 G. Kocher and N. Provatas, *Phys. Rev. Lett.*, 2015, **114**, 155501.
45 E. J. Schwalbach, J. A. Warren, K.-A. Wu and P. W. Voorhees, *Phys. Rev. E: Stat., Nonlinear, Soft Matter Phys.*, 2013, **88**, 023306.
46 A. P. Gast and Y. Monovoukas, *Nature*, 1991, **351**, 553.
47 G. Tegze, L. Gránásy, G. I. Tóth, F. Podmaniczky, A. Jaatinen, T. A. Nissila and T. Pusztai, *Phys. Rev. Lett.*, 2009, **103**, 035702.
48 K. Q. Zhang and X. Y. Liu, *Nature*, 2004, **429**, 6993.
49 X. Y. Liu, K. Maiwa and K. Tsukamoto, *J. Chem. Phys.*, 1997, **106**, 1870.
50 S. L. Girshickl and C. P. Chiu, *J. Chem. Phys.*, 1990, **93**, 1273.